Letter | Editors' Suggestion

Electron-phonon coupling in the charge density wave state of CsV_3Sb_5

Yaofeng Xie,[1,*] Yongkai Li,[2,3,4,*] Philippe Bourges,[5,†] Alexandre Ivanov,[6] Zijin Ye,[7] Jia-Xin Yin,[8] M. Zahid Hasan,[8,9,10] Aiyun Luo,[7] Yugui Yao,[2,3] Zhiwei Wang,[2,3,4,‡] Gang Xu,[7,§] and Pengcheng Dai[1,‖]

[1]*Department of Physics and Astronomy, Rice University, Houston, Texas 77005, USA*

[2]*Centre for Quantum Physics, Key Laboratory of Advanced Optoelectronic Quantum Architecture and Measurement (MOE), School of Physics, Beijing Institute of Technology, Beijing 100081, China*

[3]*Beijing Key Lab of Nanophotonics and Ultrafine Optoelectronic Systems, Beijing Institute of Technology , Beijing 100081, China*

[4]*Material Science Center, Yangtze Delta Region Academy of Beijing Institute of Technology, Jiaxing, 314011, China*

[5]*Laboratoire Léon Brillouin, CEA-CNRS, Université Paris-Saclay, CEA Saclay, 91191 Gif-sur-Yvette, France*

[6]*Institut Laue-Langevin, 71 avenue des Martyrs CS 20156, 38042 Grenoble Cedex 9, France*

[7]*Wuhan National High Magnetic Field Center & School of Physics, Huazhong University of Science and Technology, Wuhan 430074, China*

[8]*Laboratory for Topological Quantum Matter and Advanced Spectroscopy (B7), Department of Physics, Princeton University, Princeton, New Jersey 08544, USA*

[9]*Princeton Institute for Science and Technology of Materials, Princeton University, Princeton, New Jersey 08544, USA*

[10]*Materials Sciences Division, Lawrence Berkeley National Laboratory, Berkeley, California 94720, USA*

(Received 31 October 2021; accepted 23 March 2022; published 5 April 2022)

Metallic materials with kagome lattice structure are interesting because their electronic structures can host flat bands, Dirac cones, and van Hove singularities, resulting in strong electron correlations, nontrivial band topology, charge density wave (CDW), and unconventional superconductivity. Recently, kagome lattice compounds AV_3Sb_5 (A = K, Rb, Cs) are found to have intertwined CDW order and superconductivity. The origin of the CDW has been suggested to arise from Fermi-surface instabilities of van Hove singularity (saddle point) near the M points with weak electron-phonon coupling. Here we use neutron scattering experiments to demonstrate that the CDW order in CsV_3Sb_5 is associated with static lattice distortion and a sudden hardening of the B_{3u} longitudinal optical phonon mode at the Brillouin zone boundary, thus establishing that the wave vector dependent electron-phonon coupling must also play an important role in the CDW order of AV_3Sb_5.

DOI: 10.1103/PhysRevB.105.L140501

Two-dimensional (2D) correlated transition metal materials with nearly square lattice structures have been heavily investigated because they display exotic properties such as unconventional superconductivity, electronic nematic phase, and intertwined charge, spin, and lattice order [1,2]. The 2D kagome lattice metallic materials, where atoms are arranged into layered sets of corner-sharing triangles [3], are interesting because their electronic structures can host flat bands with quenched kinetic energy [4–7], Dirac cones [8,9], and van Hove singularities, resulting in strong electron correlations, nontrivial band topology, charge density wave (CDW) [10–12], and unconventional superconductivity [13,14]. Recently, CDW order and superconductivity have been discovered to coexist in kaogme lattice metals AV_3Sb_5 (A = K, Rb, Cs) [Figs. 1(a) and 1(b)] [14–16]. In general, CDW order may originate from Fermi-surface instability following the Peierls' description of an electronic instability in a one-dimensional (1D) chain of atoms [17–20] or strong electron-phonon coupling (EPC)/electron-electron correlations [21–23]. Using inelastic x-ray scattering and angle resolved photoemission spectroscopy (ARPES), it was found that the CDW here has a three-dimensional (3D) CDW order with $2 \times 2 \times 2$ superstructure but fails to induce acoustic phonon anomalies at the CDW wave vector [24]. These results are consistent with the notion that CDW in AV_3Sb_5 arises from Fermi-surface instabilities of van Hove singularity (saddle point) near the Brillouin zone boundary M points [Figs. 1(c) and 2(a)] [25,26]. If this is indeed the case [27], the CDW order and superconductivity may intertwine in AV_3Sb_5 to form the exotic roton pair-density wave superconductivity and Majorana zero mode [16,28,29]. Therefore, to understand the electron pairing mechanism of superconductivity in AV_3Sb_5, one must first unveil the microscopic origin of the CDW order.

The absence of acoustic phonon anomalies in the charge ordered state of AV_3Sb_5 from x-ray scattering experiments suggests a weak EPC [24]. However, recent ARPES [30] and optical spectroscopy [31] measurements in AV_3Sb_5 suggest that wave vector dependent EPC plays an important role in inducing the CDW transition. Since neutrons cannot detect translational symmetry-breaking electron charge distribution but are sensitive to lattice distortion and phonon anomaly induced by the CDW order, we use neutron scattering to confirm

*These authors contributed equally to this work.
†philippe.bourges@cea.fr
‡zhiweiwang@bit.edu.cn
§gangxu@hust.edu.cn
‖pdai@rice.edu

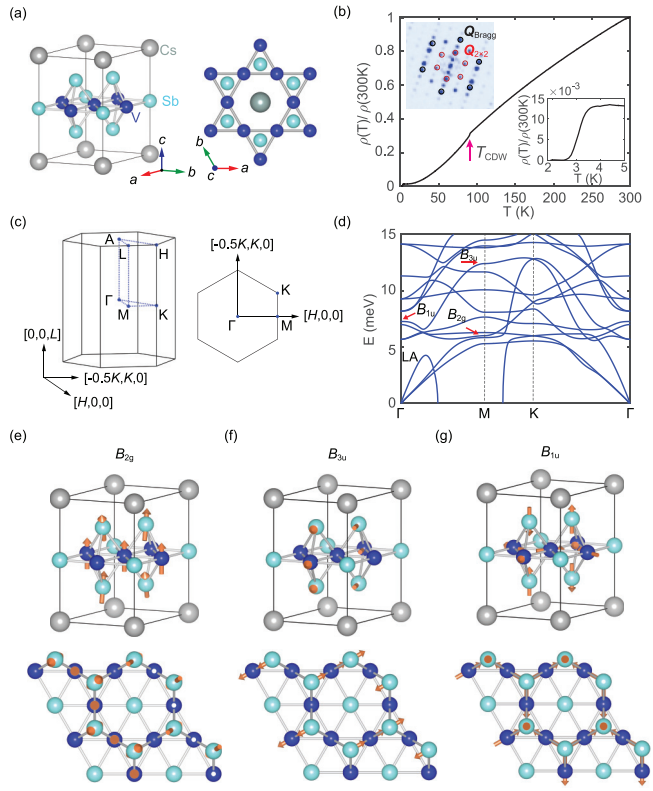

FIG. 1. (a) Crystal structure of CsV_3Sb_5 from three-dimensional view (left) and top view (right). (b) Temperature dependence of resistivity of CsV_3Sb_5, where CDW order is seen around 95 K marked by the arrow. The upper inset is the Fourier transform of Sb topographic image from STM measurement, showing the ordering peaks ($Q_{2\times2}$) and Bragg peaks (Q_{Bragg}) [15]. The lower inset shows superconducting transition temperature of the sample. (c) 3D and 2D Brillouin zone of CsV_3Sb_5. The high symmetry points are specified. (d) The DFT calculated phonon spectra of CsV_3Sb_5. The B_{2g} and B_{3u} modes at the M point with D_{2h} symmetry and the B_{1u} mode at the Γ point with D_{6h} symmetry are labeled. (e)–(g) The lattice distortion for the B_{2g}, B_{3u}, and B_{1u} modes in 3D view (left) and top view (right), respectively.

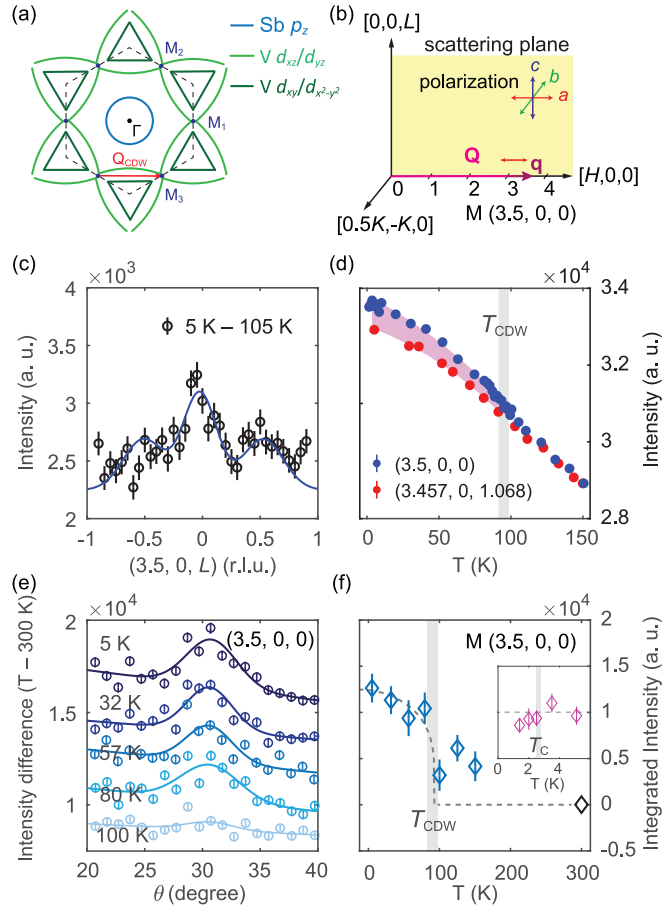

FIG. 2. (a) Schematics of the Fermi surface of CsV_3Sb_5, where the circular Fermi surface near Γ is from Sb p_z band, and vanadium d_{xz}/d_{yz} and $d_{xy}/d_{x^2-y^2}$ bands are shown in light and dark green, respectively [14,26,30]. The CDW order is suggested to be associated with Fermi surface instability of the M points (red arrow). (b) Schematics of the $[H, 0, L]$ scattering plane. The double-headed arrows represent the phonon polarization directions. For wave vectors probed in the present experiment, we are mostly probing longitudinal phonon modes along the Γ-M (H) direction. (c) The temperature difference elastic scattering along the $[3.5, 0, L]$ direction. The raw data are shown in the Supplemental Material [36]. The solid line is the Gaussian fit to the data. (d) Temperature dependence of the scattering at (3.5,0,0) and (3.475,0,1.068) positions [36]. (e) Temperature differences of rocking curve scans across $\mathbf{Q} = (3.5, 0, 0)$ using 300 K data as background. The solid lines are Gaussian fits to the data. (f) Temperature dependence of the integrated intensity at (3.5,0,0) across the T_{CDW}. The inset shows temperature dependence of the CDW order integrated intensity across T_c.

the charge order and search for phonon anomaly across the CDW order temperature.

In this paper, we report elastic and inelastic neutron scattering studies of CsV_3Sb_5, which exhibits CDW order at $T_{CDW} = 94$ K and superconductivity at $T_c = 2.5$ K [14]. We observe in-plane 2×2 superlattice peak below $T_{CDW} = 94$ K, thus confirming the x-ray scattering results [14,24]. However, we find no detectable changes in charge ordering intensity across T_c. Furthermore, we use inelastic neutron scattering to map out longitudinal acoustic and optical phonon modes near Bragg peak position (3,0,0) (zone center Γ point) at temperatures across T_{CDW} and T_c (Figs. 1–4). While acoustic phonon mode show no dramatic change across T_{CDW} consistent with the earlier work [24], we find that the optical B_{3u} phonon mode with D_{2h} symmetry [Figs. 1(d) and 1(f)], associated with the 2×2 charge order and inverse Star of David deformation of the kagome lattice [32–35], hardens across T_{CDW} at the M point. We also identified an optical B_{1u} phonon mode near the expected energy with the D_{6h} symmetry at the Γ point [Fig. 1(d)], and found it to have no observable changes across T_{CDW}. Therefore, our results firmly establish that the CDW order in CsV_3Sb_5 is associated with wave vector dependent EPC and optical phonon modes coupled with inverse Star of David deformation of the kagome lattice.

Our neutron scattering experiments were carried out at the IN8 thermal triple-axis spectrometer at the Institut Laue-Langevin (ILL), Grenoble, France. We used doubly focused pyrolytic graphite monochromator and analyzer with

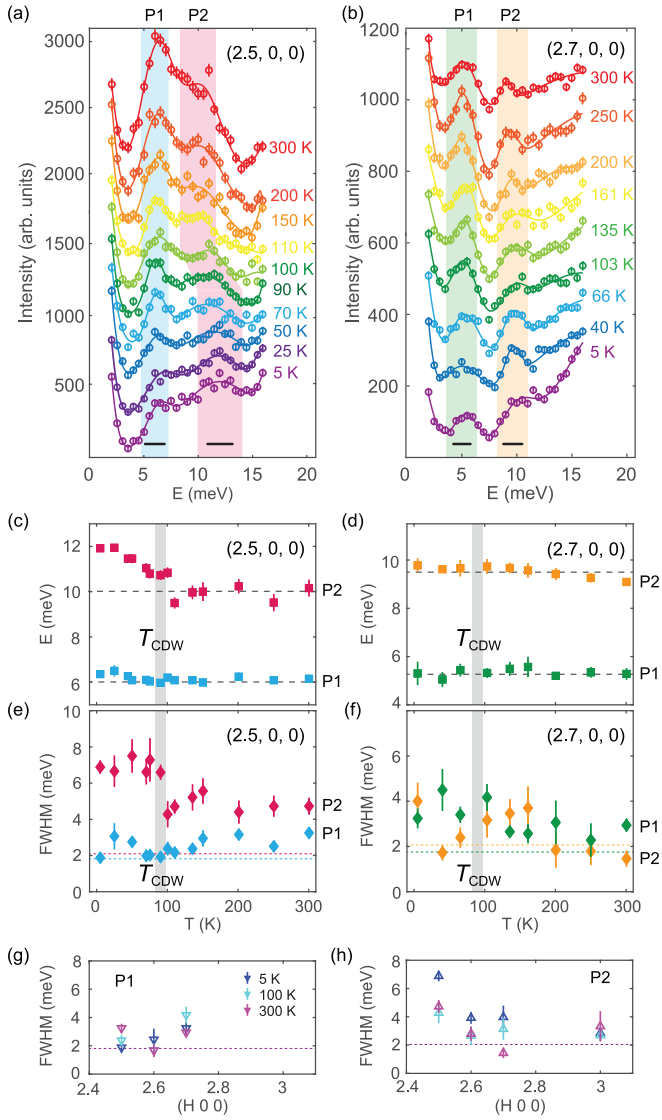

FIG. 3. (a) and (b) Temperature dependence of the constant-**Q** scans at $\mathbf{Q} = (2.5, 0, 0)$ and (2.7,0,0), respectively. The color-shaded regions highlight the two peaks, P1 and P2, observed by inelastic neutron scattering. Solid lines are results from multiple Gaussian fits. The scans are shifted vertically for clarity. The horizontal bars indicate instrumental energy resolution at different energies. (c) and (d) Temperature dependence of the phonon energy at (2.5,0,0) and (2.7,0,0), respectively. The phonon mode at $\mathbf{Q} = (2.5, 0, 0)$ hardens below T_{CDW}. (e) and (f) Temperature dependent phonon energy linewidths of the P1 and P2 mode at (2.5,0,0) and (2.7,0,0), respectively. (g) and (h) Wave vector dependence of the phonon linewidths of the P1 and P2 modes, respectively. The shaded vertical bars in (c)–(f) mark the temperature of CDW order in CsV_3Sb_5 and horizontal dashed lines are guides to the eye. The horizontal dashed lines in (c)–(h) indicate the instrumental resolution.

PG(0,0,2) reflection and fixed scattered (final) energy $E_f = 14.68$ meV. Several scans have been performed with a 2D-focusing Si(1,1,1) monochromator. Using a hexagonal lattice with $a = b = 5.495$ Å, $c = 9.309$ Å as shown in Fig. 1(a) to describe its crystal structure, the momentum transfer $\mathbf{Q} = H\mathbf{a}^* + K\mathbf{b}^* + L\mathbf{c}^*$ is denoted as (H, K, L) in reciprocal lattice units (r.l.u.) [Fig. 1(c)] [14]. About 400 individual single crystals were co-aligned on four aluminum plates to form an assembly with a volume of 0.11 cm^3 and an in-plane mosaic spread of 3.5 deg [36]. The crystal assembly was put inside a He cryostat and oriented in the $[H, 0, L]$ horizontal scattering plane. We also use density functional theory (DFT) to calculate the phonon spectra similarly to previous work [32].

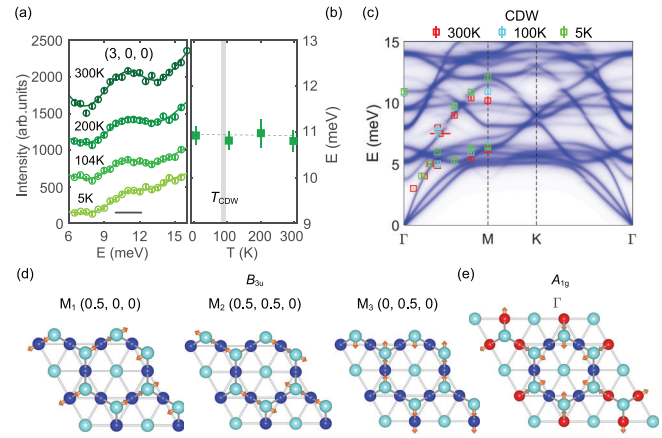

FIG. 4. (a) Temperature dependence of the constant-**Q** scans at (3,0,0), where a phonon mode at 11 meV is seen. The solid lines are Gaussian fits to the data. The scans are shifted vertically for clarity and the horizontal bar is the instrumental energy resolution. (b) Temperature dependence of the phonon mode energy at (3,0,0). (c) Comparison of the DFT calculated phonon spectra in the CDW phase with inelastic neutron scattering determined phonon dispersions measured at 5, 100, and 300 K. The calculation is unfolded to the non-CDW phase to compare with the neutron data. (d) Vadanium B_{3u} vibrational mode with the D_{2h} symmetry at three M positions. (e) Sum of the three B_{3u} mode has the A_{1g} symmetry at the Γ point in the CDW state.

Figure 1(b) shows transport data for CsV_3Sb_5, confirming the existence of CDW order below $T_{CDW} = 95$ K and superconductivity below $T_c \approx 2.5$ K. Previous scanning tunneling microscopy results showing 2×2 charge ordering is shown in the upper inset [15]. Figures 1(d)–1(g) summarize DFT calculated phonon spectra at ambient pressure and the symmetries of the most interesting phonon modes at the M [(0.5,0,0)] and Γ [(0,0,0)] points in reciprocal space. Consistent with previous work [32], we find that the longitudinal acoustic phonon mode is unstable at ambient pressure, suggesting that this mode may be relevant to the formation of CDW order. At the M point we expect to observe optical B_{2g} and B_{3u} phonon modes with the D_{2h} symmetry, corresponding to out-of-plane and half-breathing mode of vanadium as shown in Figs. 1(e) and 1(f), respectively.

Figure 2 summarizes the key results from our neutron diffraction experiments to probe the temperature dependence of the lattice distortion induced by the CDW order. From ARPES experiments, it was found that the electronic structure of of AV_3Sb_5 is dominated by vanadium bands near M points [Fig. 2(a)] [14,25,26,30,37]. Therefore, the 2×2 CDW order may arise from Fermi surface nesting of quasiparticle excitations between the three M points. Since our crystal assembly is aligned in the $[H, 0, L]$ scattering zone [Fig. 2(b)], we can

probe elastic scattering as well as phonons around nuclear Bragg peak (3,0,0) position and compare the outcome with x-ray scattering experiments [24]. Figure 2(c) shows temperature difference plot of the $[3.5, 0, L]$ elastic scan between 5 and 100 K. We find a clear peak centered at $L = 0$ and weaker peaks at $L = \pm 0.5$, thus establishing the presence of low-temperature lattice distortion in CsV_3Sb_5. To confirm that the temperature dependent lattice distortion is associated with the CDW order [14–16,24], we measure temperature dependence of the scattering at the (3.5,0,0) (signal) and (3.457,0,1.068) (background) positions, revealing clear intensity gain of the (3.5,0,0) scattering approximately below T_{CDW} [Fig. 2(d)]. Figure 2(e) shows rocking curve scans around (3.5,0,0) at temperatures across T_{CDW} using 300 K data as background scattering. While the scattering is featureless at 100 K, a clear peak centered at (3.5,0,0) appears at temperatures below T_{CDW} [Fig. 2(e)]. Figure 2(f) shows temperature dependence of the integrated intensity, again confirming the appearance of the CDW peak below T_{CDW}. However, the intensity of CDW peak does not seem to change across the superconducting transition temperature T_c [see inset of Fig. 2(f)]. The CDW (3.5,0,0) peak has an integrated intensity of $\sim 1.8 \times 10^{-4}$ of the nearby Bragg peak (3,0,0). Therefore, the intensity of the CDW peak observed by neutrons is very similar than that of x-ray experiments [24,36], suggesting that both techniques see the same lattice distortion even though their scattering amplitudes are rather different.

Figures 3(a) and 3(b) show constant-$\mathbf{Q}$ scans at $\mathbf{Q} = (2.5, 0, 0)$ (the M point) and (2.7,0,0) (approximate middle of the Brillouin zone), respectively, from room temperature to 5 K across T_{CDW}. These scans show two weakly dispersive phonon modes at $E \approx 6$ and ~ 10 meV. While the ~ 10 meV mode at the M point shows a clear ~ 2 meV hardening below T_{CDW}, the ~ 6 meV mode only hardens slightly on cooling, and has negligible changes across T_{CDW} [Fig. 3(c)]. In addition, the full-width half-maximum (FWHM) of the ~ 10 meV mode is clearly broader than the instrumental resolution [horizontal bars in Figs. 3(a) and 3(b)] and broadens further below T_{CDW}, but the ~ 6 meV mode is basically resolution limited and changes negligibly across T_{CDW} [Fig. 3(e)]. For comparison, these two phonon modes at $\mathbf{Q} = (2.7, 0, 0)$ show no observable anomaly across T_{CDW} in energy position [Fig. 3(d)] and width [Fig. 3(f)]. The wave vector dependence of the FWHM of the ~ 6 and ~ 10 meV modes at temperatures above (100 and 300 K) and below (5 K) T_{CDW} is shown in Figs. 3(g) and 3(h). Consistent with Figs. 3(a)–3(f), the ~ 10 meV mode shows clear broadening below T_{CDW} at the M point. These results suggest wave vector dependent EPC in CsV_3Sb_5, as seen other CDW materials [38,39].

Figure 4(a) shows constant-$\mathbf{Q}$ scans at the $\mathbf{Q} = (3, 0, 0)$ position below and above T_{CDW}. While the data shows an instrumental resolution-limited phonon mode at $E \approx 11$ meV, both the mode energy and FWHM reveal no obvious changes across T_{CDW} [Fig. 4(b)], suggesting that the mode is not affected by the CDW order. Figure 4(c) shows the DFT phonon spectra calculated first by using the experimental 2×2 CDW structure at ambient pressure and then unfolding the results into the Brillouin zone of the pristine cell to facilitate comparison with the neutron results [40]. From the lattice cross section of neutron scattering, we can only measure phonon branches with the polarization direction parallel to the momentum transfer $\mathbf{Q}$ [41]. This means that within the experimental setup of the $[H, 0, L]$ scattering plane, we only detect the longitudinal phonon modes with vibrations along the Γ-M direction. Figure 4(c) compares the measured and calculated dispersion curves for CsV_3Sb_5. Inspection of the figure reveals that the measured longitudinal acoustic phonon mode agrees with the DFT calculation unfolded in the CDW state reasonably well. This means that the energy of the zone boundary longitudinal acoustic phonon mode occurs at approximately 6 meV. Since our instrumental energy resolution is on the order of 1.5 meV, we are sensitive to any acoustic phonon changes above 2 meV. Instead, we find no evidence of the acoustic phonon mode softening at the M point in the CDW state [Fig. 3(c)], consistent with the inelastic x-ray scattering work [24]. On the other hand, the optical phonon mode at ~ 10 meV is likely associated with the half-breathing mode of vanadium with the B_{3u} symmetry [Fig. 4(c)].

As discussed in Ref. [23], the classical picture of Fermi surface nesting induced CDW order from Peierls' description [17,18] fails in many real systems and the wave vector dependence of the EPC matrix element determines the characteristic of the CDW phase. For example, CDW order in $NbSe_2$ is not due to Fermi surface nesting but instead arises from the EPC as it is seen phonon energy softening, broadened phonon linewidth at the CDW ordering wave vector [23]. The situation in CsV_3Sb_5 is somewhat different. While there is no evidence of acoustic phonon softening and broadening at the charge ordering wave vector (Figs. 3 and 4) consistent with the weakly first order nature of the CDW transition [14,24], the energy of optical phonon B_{3u} mode shows a clear hardening below T_{CDW} [Fig. 3(c)]. In addition, the optical phonon linewidth broadens at the CDW wave vector below T_{CDW} [Fig. 3(h)]. Since charge order occurs at three equivalent M points, superposition of three B_{3u} modes by band folding in the CDW state can lead to a vanadium breathing A_{1g} mode and two other degenerate modes that do not have threefold rotational symmetry at the Γ point (D_{6h} symmetry) [Figs. 4(d) and 4(e)]. The former corresponds to an inverse Star of David deformation of vanadium atoms. Therefore, our experimental results, not predicted by any theory, provide strong evidence that wave vector dependent EPC must play an important role in the formation of the CDW order in CsV_3Sb_5, consistent with recent first-principles studies of the CDW order in CsV_3Sb_5 [42,43]. In addition, these results will provide quantitative constraints on future theories of the EPC and CDW order in CsV_3Sb_5. Although recent μSR measurements suggest that CDW order is also associated with a time reversal symmetry breaking field [44], consistent with the presence of a chiral flux phase in the CDW state of CsV_3Sb_5 [45,46], it is unclear how the time reversal symmetry breaking field in the CDW state induced by flux phase can affect the lattice and its vibrations.

In summary, we have carried out elastic and inelastic neutron scattering experiments on CsV_3Sb_5. Our elastic results confirm the presence of 2 by 2 charge order below 95 K [14,24]. By comparing phonons measured by inelastic neutron scattering experiments with that of DFT calculations, we conclude that acoustic phonons in CsV_3Sb_5 do not respond to CDW order but optical B_{3u} phonon mode with the D_{2h}

symmetry hardens below T_{CDW} at M points. This phonon hardening is likely associated with an inverse Star of David deformation of vanadium atoms with the A_{1g} breathing mode at the Γ point [32]. These results therefore indicate that the effect of wave vector dependent EPC must be taken into account to achieve a comprehensive understanding of the CDW state in AV_3Sb_5.

P.D. is grateful to Binghai Yan, B. R. Ortiz, and Stephen Wilson for helpful discussions. The neutron scattering and basic materials characterization work at Rice is supported by the U.S. DOE, BES under Grant No. DE-SC0012311 and by the Robert A. Welch Foundation under Grant No. C-1839, respectively (P.D.). The work at Beijing Institute of Technology was supported by the National Key R&D Program of China (Grant No. 2020YFA0308800), the Natural Science Foundation of China (Grants No. 92065109 and No. 11734003), the Beijing Natural Science Foundation (Grants No. Z190006 and No. Z210006), and the Beijing Institute of Technology (BIT) Research Fund Program for Young Scholars (Grant No. 3180012222011). Z.W. thanks the Analysis & Testing Center at BIT for assistance in facility support. Work at Huazhong University of Science and Technology was supported by the National Key Research and Development Program of China (2018YFA0307000), and the National Natural Science Foundation of China (11874022). Materials characterization and the study of topological quantum properties were supported by the U.S. Department of Energy, Office of Science, National Quantum Information Science Research Centers, Quantum Science Center and Princeton University (M.Z.H.).

[1] E. Fradkin, S. A. Kivelson, and J. M. Tranquada, Rev. Mod. Phys. **87**, 457 (2015).
[2] P. C. Dai, Rev. Mod. Phys. **87**, 855 (2015).
[3] I. Syôzi, Prog. Theor. Phys. **6**, 306 (1951).
[4] B. Sutherland, Phys. Rev. B **34**, 5208 (1986).
[5] D. Leykam, A. Andreanov, and S. Flach, Adv. Phys.: X **3**, 1473052 (2018).
[6] I. I. Mazin, H. O. Jeschke, F. Lechermann, H. Lee, M. Fink, R. Thomale, and R. Valentí, Nat. Commun. **5**, 4261 (2014).
[7] J.-X. Yin, S. S. Zhang, G. Chang, Q. Wang, S. S. Tsirkin, Z. Guguchia, B. Lian, H. Zhou, K. Jiang, I. Belopolski, N. Shumiya, D. Multer, M. Litskevich, T. A. Cochran, H. Lin, Z. Wang, T. Neupert, S. Jia, H. Lei, and M. Z. Hasan, Nat. Phys. **15**, 443 (2019).
[8] L. Ye, M. Kang, J. Liu, F. von Cube, C. R. Wicker, T. Suzuki, C. Jozwiak, A. Bostwick, E. Rotenberg, D. C. Bell, L. Fu, R. Comin, and J. G. Checkelsky, Nature (London) **555**, 638 (2018).
[9] J.-X. Yin, S. S. Zhang, H. Li, K. Jiang, G. Chang, B. Zhang, B. Lian, C. Xiang, I. Belopolski, H. Zheng, T. A. Cochran, S.-Y. Xu, G. Bian, K. Liu, T.-R. Chang, H. Lin, Z.-Y. Lu, Z. Wang, S. Jia, W. Wang, and M. Zahid Hasan, Nature (London) **562**, 91 (2018).
[10] S.-L. Yu and J.-X. Li, Phys. Rev. B **85**, 144402 (2012).
[11] W.-S. Wang, Z.-Z. Li, Y.-Y. Xiang, and Q.-H. Wang, Phys. Rev. B **87**, 115135 (2013).
[12] M. L. Kiesel, C. Platt, and R. Thomale, Phys. Rev. Lett. **110**, 126405 (2013)
[13] B. R. Ortiz, L. C. Gomes, J. R. Morey, M. Winiarski, M. Bordelon, J. S. Mangum, I. W. H. Oswald, J. A. Rodriguez-Rivera, J. R. Neilson, S. D. Wilson, E. Ertekin, T. M. McQueen, and E. S. Toberer, Phys. Rev. Material **3**, 094407 (2019).
[14] B. R. Ortiz, S. M. L. Teicher, Y. Hu, J. L. Zuo, P. M. Sarte, E. C. Schueller, A. M. M. Abeykoon, M. J. Krogstad, S. Rosenkranz, R. Osborn, R. Seshadri, L. Balents, J. He, and S. D. Wilson, Phys. Rev. Lett. **125**, 247002 (2020).
[15] Y.-X. Jiang, J.-X. Yin, M. Michael Denner, N. Shumiya, B. R. Ortiz, G. Xu, Z. Guguchia, J. He, Md. S. Hossain, X. Liu, J. Ruff, L. Kautzsch, S. S. Zhang, G. Chang, I. Belopolski, Q. Zhang, T. A. Cochran, D. Multer, M. Litskevich, Z.-J. Cheng, X. P. Yang, Z. Wang, R. Thomale, T. Neupert, M. Zahid Hasan *et al.*, Nat. Mater. **20**, 1353 (2021).
[16] Z. Liang, X. Hou, F. Zhang, W. Ma, P. Wu, Z. Zhang, F. Yu, J.-J. Ying, K. Jiang, L. Shan, Z. Wang, and X.-H. Chen, Phys. Rev. X **11**, 031026 (2021).
[17] R. E. Peierls, *Quantum Theory of Solids* (Oxford University Press, New York, 1955).
[18] W. Kohn, Phys. Rev. Lett. **2**, 393 (1959).
[19] T. M. Rice and G. K. Scott, Phys. Rev. Lett. **35**, 120 (1975).
[20] M. D. Johannes, I. I. Mazin, and C. A. Howells, Phys. Rev. B **73**, 205102 (2006).
[21] J. Zaanen and O. Gunnarsson, Phys. Rev. B **40**, 7391 (1989).
[22] C. M. Varma and A. L. Simons, Phys. Rev. Lett. **51**, 138 (1983).
[23] X. Zhu, Y. Cao, J. Zhang, E. W. Plummer, and J. Guo, Proc. Natl. Acad. Sci. USA **112**, 2367 (2015).
[24] H. Li, T. T. Zhang, T. Yilmaz, Y. Y. Pai, C. E. Marvinney, A. Said, Q. W. Yin, C. S. Gong, Z. J. Tu, E. Vescovo, C. S. Nelson, R. G. Moore, S. Murakami, H. C. Lei, H. N. Lee, B. J. Lawrie, and H. Miao, Phys. Rev. X **11**, 031050 (2021).
[25] Z. Liu, N. Zhao, Q. Yin, C. Gong, Z. Tu, M. Li, W. Song, Z. Liu, D. Shen, Y. Huang, K. Liu, H. Lei, and S. Wang, Phys. Rev. X **11**, 041010 (2021).
[26] M. Kang, S. Fang, J.-K. Kim, B. R. Ortiz, J. Yoo, B.-G. Park, S. D. Wilson, J.-H. Park, and R. Comin, Nat. Phys. **18**, 301 (2022).
[27] T. Park, M. Ye, and L. Balents, Phys. Rev. B **104**, 035142 (2021).
[28] H. Chen, H. Yang, B. Hu, Z. Zhao, J. Yuan, Y. Xing, G. Qian, Z. Huang, G. Li, Y. Ye, S. Ma, S. Ni, H. Zhang, Q. Yin, C. Gong, Z. Tu, H. Lei, H. Tan, S. Zhou, C. Shen, X. Dong, B. Yan, H.-J. Gao *et al.*, Nature (London) **599**, 222 (2021).
[29] H. Zhao, H. Li, B. R. Ortiz, S. M. L. Teicher, T. Park, M. Ye, Z. Wang, L. Balents, S. D. Wilson, and I. Zeljkovic, Nature (London) **599**, 216 (2021).
[30] H. Luo, Q. Gao, H. Liu, Y. Gu, D. Wu, C. Yi, J. Jia, S. Wu, X. Luo, Y. Xu, L. Zhao, Q. Wang, H. Mao, G. Liu, Z. Zhu, Y. Shi, K. Jiang, J. Hu, Z. Xu, and X. J. Zhou, Nat. Commun. **13**, 273 (2022).
[31] E. Uykur, B. R. Ortiz, S. D. Wilson, M. Dressel, and A. A. Tsirlin, npj Quantum Mater. **7**, 16 (2022).

[32] H. Tan, Y. Liu, Z. Wang, and B. Yan, Phys. Rev. Lett. **127**, 046401 (2021).

[33] B. R. Ortiz, S. M. L. Teicher, L. Kautzsch, P. M. Sarte, N. Ratcliffe, J. Harter, J. P. C. Ruff, R. Seshadri, and S. D. Wilson, Phys. Rev. X **11**, 041030 (2021).

[34] N. Ratcliff, L. Hallett, B. R. Ortiz, S. D. Wilson, and J. W. Harter, Phys. Rev. Material **5**, L111801 (2021).

[35] H. Miao, H. X. Li, W. R. Meier, A. Huon, H. N. Lee, A. Said, H. C. Lei, B. R. Ortiz, S. D. Wilson, J. X. Yin, M. Z. Hasan, Z. Wang, H. Tan, and B. Yan, Phys. Rev. B **104**, 195132 (2021).

[36] See Supplemental Material at http://link.aps.org/supplemental/10.1103/PhysRevB.105.L140501 for raw data and additional discussion which includes Z. Wang, Y.-X. Jiang, J.-X. Yin, Y. Li, G.-Y. Wang, H.-L. Huang, S. Shao, J. Liu, P. Zhu, N. Shumiya *et al.*, Phys. Rev. B 104, 075148 (2021).

[37] Z. Wang, S. Ma, Y. Zhang, H. Yang, Z. Zhao, Y. Ou, Y. Zhu, S. Ni, Z. Lu, H. Chen, K. Jiang, L. Yu, Y. Zhang, X. Dong, J. Hu, H.-J. Gao, and Z. Zhao, arXiv:2104.05556.

[38] F. Weber, S. Rosenkranz, J.-P. Castellan, R. Osborn, R. Hott, R. Heid, K.-P. Bohnen, T. Egami, A. H. Said, and D. Reznik, Phys. Rev. Lett. **107**, 107403 (2011).

[39] M. Maschek, S. Rosenkranz, R. Heid, A. H. Said, P. Giraldo-Gallo, I. R. Fisher, and F. Weber, Phys. Rev. B **91**, 235146 (2015).

[40] Y. Ikeda, A. Carreras, A. Seko, A. Togo, and I. Tanaka, Phys. Rev. B **95**, 024305 (2017).

[41] A. T. Boothroyd, *Principles of Neutron Scattering from Condensed Matter* (Oxford University Press, Oxford, 2020), Chap. 8.

[42] J. F. Zhang, K. Liu, and Z. Y. Lu, Phys. Rev. B **104**, 195130 (2021).

[43] J. G. Si, W. J. Lu, Y. P. Sun, P. F. Liu, and B. T. Wang, Phys. Rev. B **105**, 024517 (2022).

[44] C. Mielke III, D. Das, J.-X. Yin, H. Liu, R. Gupta, C. N. Wang, Y.-X. Jiang, M. Medarde, X. Wu, H. C. Lei, J. J. Chang, P. Dai, Q. Si, H. Miao, R. Thomale, T. Neupert, Y. Shi, R. Khasanov, M. Z. Hasan, H. Luetkens, and Z. Guguchia, Nature (London) **602**, 245 (2022).

[45] X. Feng, K. Jiang, Z. Wang, and J. Hu, Sci. Bull. **66**, 1384 (2021).

[46] Y.-P. Lin and R. M. Nandishore, Phys. Rev. B **104**, 045122 (2021).